Journal of Power Sources 195 (2010) 4943–4951

Contents lists available at ScienceDirect

Journal of Power Sources

journal homepage: www.elsevier.com/locate/jpowsour

Elevated temperature cycling stability and electrochemical impedance of $LiMn_2O_4$ cathodes with nanoporous ZrO_2 and TiO_2 coatings

Kenneth A. Walz[a,*,1], Christopher S. Johnson[b,1], Jamie Genthe[a], Lucas C. Stoiber[a], Walter A. Zeltner[a], Marc A. Anderson[a,1], Michael M. Thackeray[b,1]

[a] Environmental Chemistry and Technology Program, University of Wisconsin-Madison, 660 N Park Street, Madison, WI 53706, United States
[b] Chemical Sciences and Engineering Division, Argonne National Laboratory, 9500 Cass Ave., Argonne, IL 60439, United States

ARTICLE INFO

Article history:
Received 6 February 2010
Received in revised form 1 March 2010
Accepted 2 March 2010
Available online 7 March 2010

Keywords:
Battery
Lithium-ion
Spinel
Coating
TiO_2
ZrO_2

ABSTRACT

In this study, nanoporous zirconia (ZrO_2) and titania (TiO_2) coatings are shown to stabilize the cycling performance of lithium-ion batteries with $LiMn_2O_4$ spinel cathodes. The effect of firing temperature on the coating pore size is discussed and the resulting performance of the coated cathodes is evaluated. Stabilization mechanisms, such as neutralization of acidic electrolytes by ZrO_2 and TiO_2 coatings, are examined. It is proposed that the establishment of a complex nanoporous network for lithium-ion transport results in a more uniform current distribution at the particle surface, thereby suppressing capacity fade that may be associated with surface instabilities of the spinel electrode.

1. Introduction

The rechargeable lithium-ion battery industry has grown tremendously in recent years with the rapid development of portable electronic devices. Lithium-ion battery chemistries are now also being prominently targeted to provide the high gravimetric and volumetric energy densities required by heavy duty applications, e.g., hybrid- and all-electric-vehicles [1–3]. Currently, $LiCoO_2$ is the dominant cathode material for these batteries. However, for mass electric-vehicle markets, global cobalt supplies may be limited; furthermore, the cost of cobalt is likely to increase significantly as demand continues to grow [4,5]. By comparison, manganese is a plentiful, inexpensive and environmentally friendly element from which the lithium-manganese-oxide spinel, $LiMn_2O_4$, can be produced as an alternative cathode material [6,7]. Many studies of $LiMn_2O_4$, including cation- and anion-substituted derivatives, have been undertaken that that have emphasized its superior safety and performance advantages over $LiCoO_2$ [8–18].

Despite advantages in terms of both cost and safety, lithium-ion cells with $LiMn_2O_4$ spinel cathodes have limitations. Chief among these is a decrease in capacity that occurs upon repeated cycling [19–21]. This problem is observable at room temperature, but is exacerbated at higher temperatures. Numerous factors have been shown to contribute to the capacity fade, such as the choice and purity of the electrolyte and the operating voltage window of the cells.

Early experiments with $Li_xMn_2O_4$spinel electrodes ($0 \le x \le 2$) showed that excessive discharge below 3.0 V resulted in the formation of $Li_2Mn_2O_4$, in which a large crystallographic (Jahn–Teller) distortion (16% change in the c/a ratio) was responsible for the capacity loss [8,22]. Non-equilibrium localized formation of $Li_2Mn_2O_4$ at the particle surface has also been observed, particularly under high rate conditions above 3 V, which can result in subsequent disproportionation reactions to yield Mn(II) and Mn(IV) products, such as MnO and Li_2MnO_3, or MnO, Li_2O and λ-MnO_2 [23–25]. Soluble Mn^{2+} ions can then be transported across the electrolyte to the carbon (graphitic) anode, where they are deposited, adversely affecting cell performance. Mn dissolution can be at least partially mitigated by cation substitution to increase the average Mn oxidation state above 3.5+ (e.g., $Li_{1+x}Mn_{2-x}O_4$) and moderating lattice parameter differences (Δa) between the charged and discharged states [23,26–28].

Electrolyte decomposition in lithium-ion cells can form Lewis acids that accelerate the decomposition of $LiMn_2O_4$, to form soluble Mn(II) species that leach into the electrolyte [29,30]. Trace amounts of water in the electrolyte can also react with fluoride-based electrolytes, generating hydrofluoric acid (HF), which has been

* Corresponding author. Tel.: +1 608 246 6521; fax: +1 608 246 6880.
E-mail address: kawalz@wisc.edu (K.A. Walz).
[1] Electrochemical Society active member.

0378-7753/$ – see front matter © 2010 Elsevier B.V. All rights reserved.
doi:10.1016/j.jpowsour.2010.03.007

implicated as an additional cause of Mn(II) dissolution [31–33]. Rotating disc electrode experiments have shown that Mn(II) dissolution occurs under both discharged (<3.1 V) and charged (>4.1 V) conditions, and is somewhat more pronounced at the higher potentials [34]. Similarly, manganese deposition on graphite anode surfaces has been documented for lithium-ion cells with $LiMn_2O_4$ spinel cathodes that were charged to 4.3 V [27].

The capacity fade of $LiMn_2O_4$ spinels has also been partially attributed to the formation of an electronically insulating solid electrolyte interface (SEI) layer that forms on the cathode surface. This process also occurs when cobalt-based cathodes are used [35], but appears to be more complex for the manganese system due to the accompanying formation of undesirable Mn products that further compromise electronic conductivity, resulting in larger polarization losses [36,37]. It has been shown that the conductivity of the SEI layer depends on the type of electrolyte employed, and that SEI formation occurs concomitantly with changes in the bulk resistance of the electrolyte [38]. Surface enhanced Raman spectroscopy has demonstrated that the SEI layer formed by the interaction of $LiMn_2O_4$ with an electrolyte of 1 M $LiPF_6$ in EC:DMC (1:1 by vol) was comprised of a complex mixture of λ-MnO_2 along with various alkoxide, carboxylic and carbonate functional groups formed by oxidation of the electrolyte [39]. It has been estimated that the capacity loss associated with the formation of the electronically insulating SEI layer is roughly double the loss that can be attributed to decomposition of the $LiMn_2O_4$ spinel electrode [40].

In recent years, various types of coatings and thin film deposition procedures have been explored to improve the electrochemical stability of $LiMn_2O_4$ cathodes in lithium cells [41–52]. For example (1) improved cycling stability was achieved by coating $LiMn_2O_4$ with MgO and Al_2O_3 precipitated from nitrate salt solutions [42]; (2) $LiMn_2O_4$ electrodes demonstrated improved stability at 55 °C when coated with ZnO to neutralize harmful acidic species in the electrolyte [43,44] and (3) we reported a stabilizing effect when amorphous ZrO_2, Al_2O_3 and SiO_2 coatings were deposited onto $LiMn_2O_4$ electrodes from colloidal suspensions using sol–gel techniques [45,46].

Despite the numerous studies in this area, a functional understanding of coated electrodes remains incomplete. It appears likely that at least some of the metal oxide coatings are capable of neutralizing acid species that might arise in the electrolyte. It has also been suggested that the coatings may act as a physical barrier to Mn(II) dissolution by forming epitaxial layers on the underlying coated spinel, or by modifying structure of the spinel surface. The coatings almost certainly have an effect on the SEI layer, which could modify the electronic- and Li^+-ion conductivity at the particle surface. At this time, it is not yet clear which of these various processes is most important to the stabilization of a $LiMn_2O_4$ electrode surface; key variables that influence coating efficacy remain to be identified and optimized for most of the coating materials that have been employed to date.

Limited information has been gathered thus far about the surface structures of coated $LiMn_2O_4$ electrodes or their stabilizing functions. Few of the studies published on this topic have reported on the morphology, heterogeneity, or pore size of the thin films, although it is well known that all of these properties can be influenced by the synthesis, deposition and sintering processes used in sol–gel chemistry [53,54]. For example, our previous studies have shown that the stabilizing effect of a ZrO_2 coating is highly dependent on particle size [46], which is likely to be one of the key parameters that determines the structure of the thin film coating, and is worthy of further characterization.

In this paper, we compare the electrochemical performance of ZrO_2- and TiO_2-coated cathodes, prepared from colloidal suspensions using sol–gel techniques, under a range of different conditions. The data are compared with physically-mixed $LiMn_2O_4$ and ZrO_2/TiO_2 composite electrodes to discern the relative contributions of acid/base neutralization and surface/interfacial effects to the stabilization of the cathode imparted by the coatings. It is highly likely that our results are relevant, not only to $LiMn_2O_4$ spinel electrodes, but also to the recently reported family of layered lithium-mixed-metal-oxides that provide exceptionally high capacities (250 mAh g^{-1}) when charged to high potentials (4.6 V) and could similarly benefit from surface stabilization [55,56].

2. Experimental

The stoichiometric lithium-manganese-oxide spinel, $LiMn_2O_4$ (Carus Corporation), which is more susceptible to surface degradation than stabilized, cation-substituted spinels such as $Li_{1+x}Mn_{2-x}O_4$ was selected for our studies to quantify the effects of ZrO_2 and TiO_2 coatings [57]. Colloidal ZrO_2- and TiO_2-suspensions were prepared via acid-catalyzed, sol–gel hydrolysis and condensation reactions of zirconium n-propoxide (Gelest) and titanium isopropoxide (Aldrich) using previously reported techniques [54]. The size of primary colloidal solid particles was determined using a ZetaSizer 3000 dynamic light scattering instrument (Malvern Inc.). Cathode materials were prepared by suspending a measured quantity of spinel in a sufficient volume of colloidal suspension to provide a 4% (by mass) coating. Details of the coating technique are described elsewhere [45,46]. The coated materials were fired for 3 h at either 300 or 400 °C with a 2 °C min^{-1} ramp rate.

To ascertain coating morphologies and the extent of surface coverage, cathode materials were inspected with a Schottky Field Emission Scanning Electron Microscope (LEO Gemini 1530). An in-lens secondary electron detector, with an accelerating voltage of 3 kV, was used to obtain high resolution surface images. To further characterize the porous coatings, sorption isotherms were measured using a Micromeritics ASAP 2010 micropore analysis instrument. Specific surface areas were estimated from Brunauer–Emmet–Teller (BET) analyses of the adsorption data at low relative pressures [58].

Cathode laminates were prepared using 84% $LiMn_2O_4$ powder mixed with 4% SFG-6 graphite (Timcal) and 4% acetylene black (Cabot) as current collecting media, and 8% polyvinylidene difluoride as binder (Kynar). The materials were mixed into a slurry using 1-methyl-2-pyrrolidinone as the suspending solvent (Aldrich). The slurry was cast onto an aluminum foil current collector using a 200 μm doctor blade. The resulting laminates were dried in air for 4 h at 75 °C at ambient pressure, followed by another 12 h under vacuum to remove any remaining solvent and adsorbed water. Two laminates were also prepared by mixing 4% (by mass) of two types of ZrO_2 powders with the $LiMn_2O_4$ spinel using a mortar and pestle in order to investigate the extent to which independent ZrO_2 particles in the electrode might neutralize acidic species in the electrolyte. The first laminate contained a commercial submicron ZrO_2 powder (Aldrich), whereas the second laminate contained a sol–gel derived ZrO_2 xerogel prepared from the same zirconium n-propoxide precursor described above. The xerogel was fired for 3 h at 400 °C, and ground separately with a mortar and pestle before it was mixed with the $LiMn_2O_4$ powder.

Laminates were pinch rolled to consolidate the dry, solid electrode powders; circular (1.6 cm^2) cathode discs were punched from these laminates. The punched cathodes were weighed to determine the amount of active spinel (typically 12–16 mg) before being loaded into sealed, stainless steel coin cells (Hohsen CR2032). A lithium foil anode (Aldrich), a tri-layered polyethylene/polypropylene separator (Celgard 2325), and an electrolyte of 1 M $LiPF_6$ dissolved in 1:1 ethylene carbonate/diethyl carbonate solvent (Merck LP-40) were used as the other cell components. Cells were assembled in a controlled atmosphere argon-filled glove

box (Vac Atmospheres) to maintain H_2O and O_2 levels below 5 ppm.

Electrochemical tests were performed using a 16 channel VMP2/Z electrochemical workstation with an impedance capability (Princeton Applied Research). Freshly assembled cells were conditioned over three, low current, break-in cycles at an approximate C/12 rate (based on a nominal anticipated capacity of 130 mAh g^{-1} for the active spinel component). The actual 'rated' capacity of each cell was then determined from the applied current and time taken to discharge the cell on the third conditioning cycle.

A series of cells was cycled at room temperature through progressively higher rates of C/10, C/5, C/2, 1 C, 2 C and 3 C (three cycles at each rate step) to determine the power capability of the ZrO_2- and TiO_2-coated electrodes versus an uncoated, 'control' spinel electrode. The high power cycles were followed by further C/10 cycles to determine the extent of capacity loss at the slowest cycling rate. A second series of cells was cycled at 1 and 3 C rates at 55 °C to determine the extent of high temperature capacity fade. Finally, impedance spectra were obtained at cell potentials of 4.00, 4.13 and 4.30 V, before and after the high temperature experiments to explore changes in the electrochemical properties of the cells under various cycling conditions. In all cases, multiple cells containing each cathode type were evaluated to determine average impedance values and standard deviations. Data analyses were performed using EC Lab 9.15 and ZSimpWin 3.20 software (PAR).

3. Results and discussion

3.1. Coating characterization

The average size of the ZrO_2 and TiO_2 particles in the colloidal suspensions (sols) was 3.3 and 4.8 nm, respectively (Fig. 1). Both sols exhibited unimodal particle size distributions with narrow peak widths. These results were consistent with earlier descriptions of these materials [54]. Pore sizes for the thin film coatings can be estimated by assuming that the coatings are formed by random close packing of spherical particles. This results in two characteristic pore types of roughly triangular and rectangular shape (Fig. 2). Based on their measured mean diameters, the 3.3 nm ZrO_2 particles would be expected to generate pore sizes ranging from about 0.5 to 1.6 nm in size, whereas the larger 4.8 nm TiO_2 particles would produce pores of 0.7–2.0 nm in size [59,60]. For scale comparison, it is useful to note that the solvated radius of the lithium-ion in

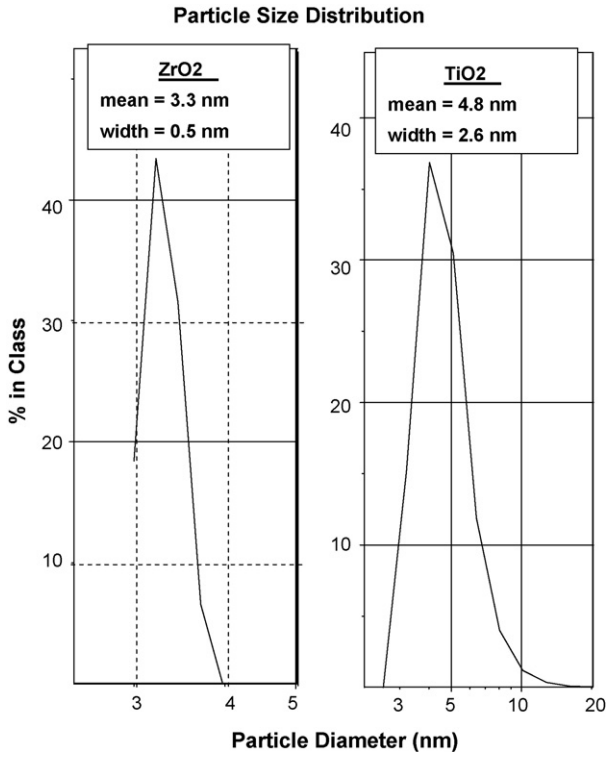

Fig. 1. Particle sizes for ZrO_2 and TiO_2 colloidal suspensions used for sol–gel coating of spinel cathodes.

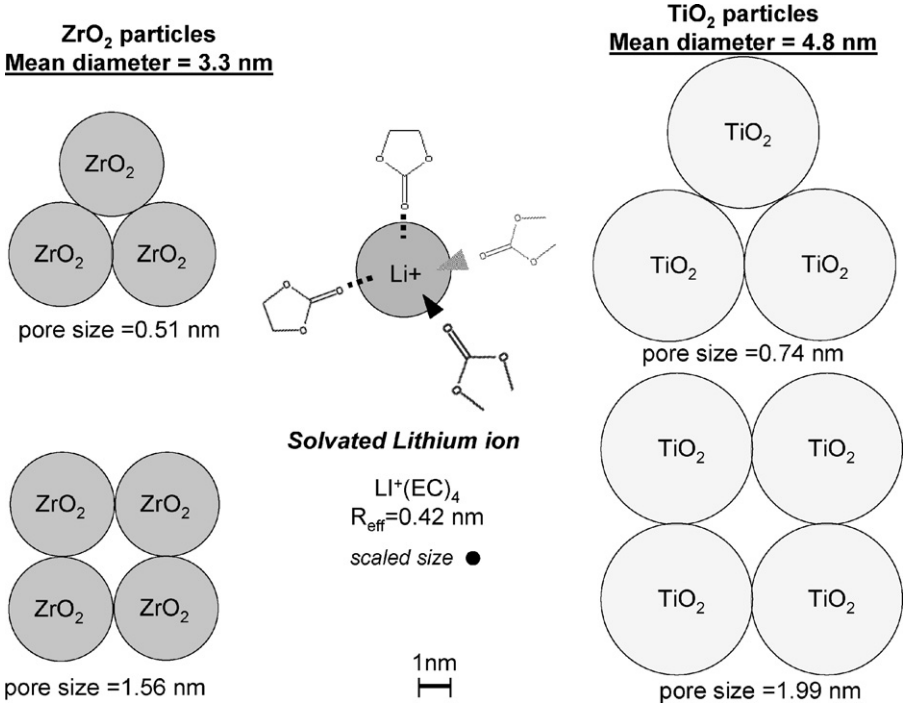

Fig. 2. Scaled representation of pore sizes resulting from random close packing arrangements of spherical ZrO_2 and TiO_2 particles relative to the solvated lithium-ion in ethylene carbonate electrolyte.

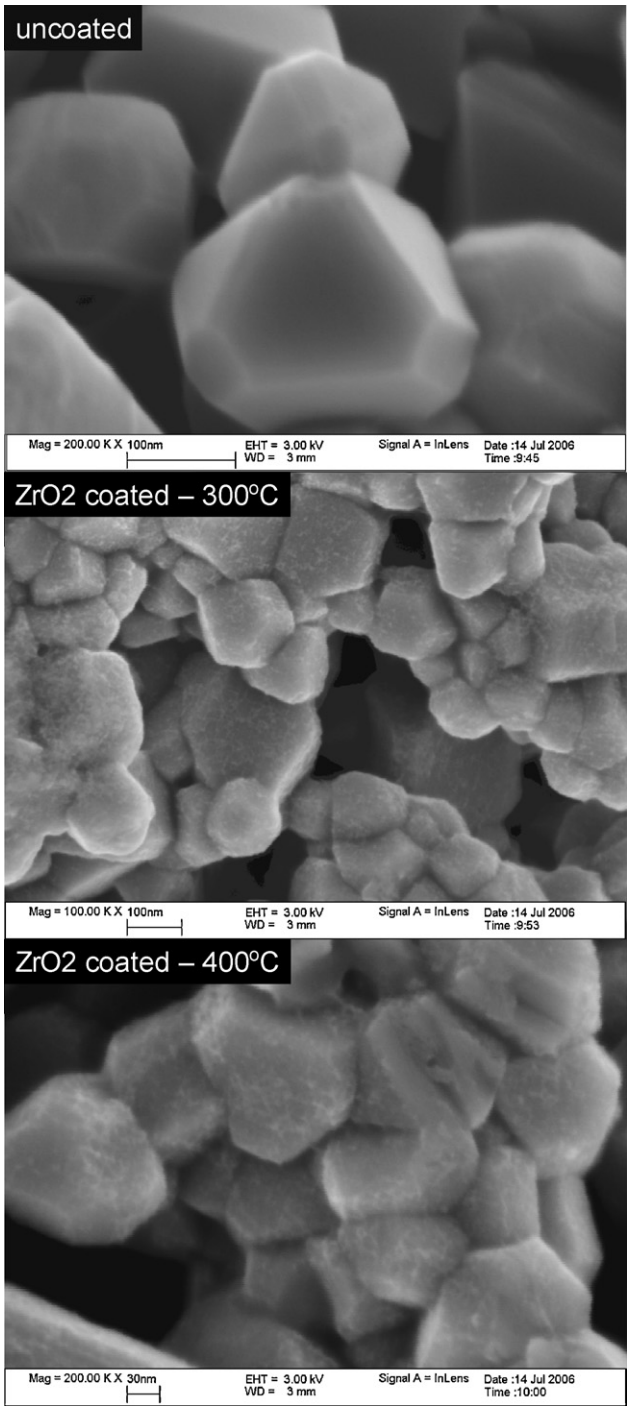

Fig. 3. SEM images of uncoated, ZrO_2-coated and TiO_2-coated electrode laminates at 20,000× (left) and 50,000× (right) magnification.

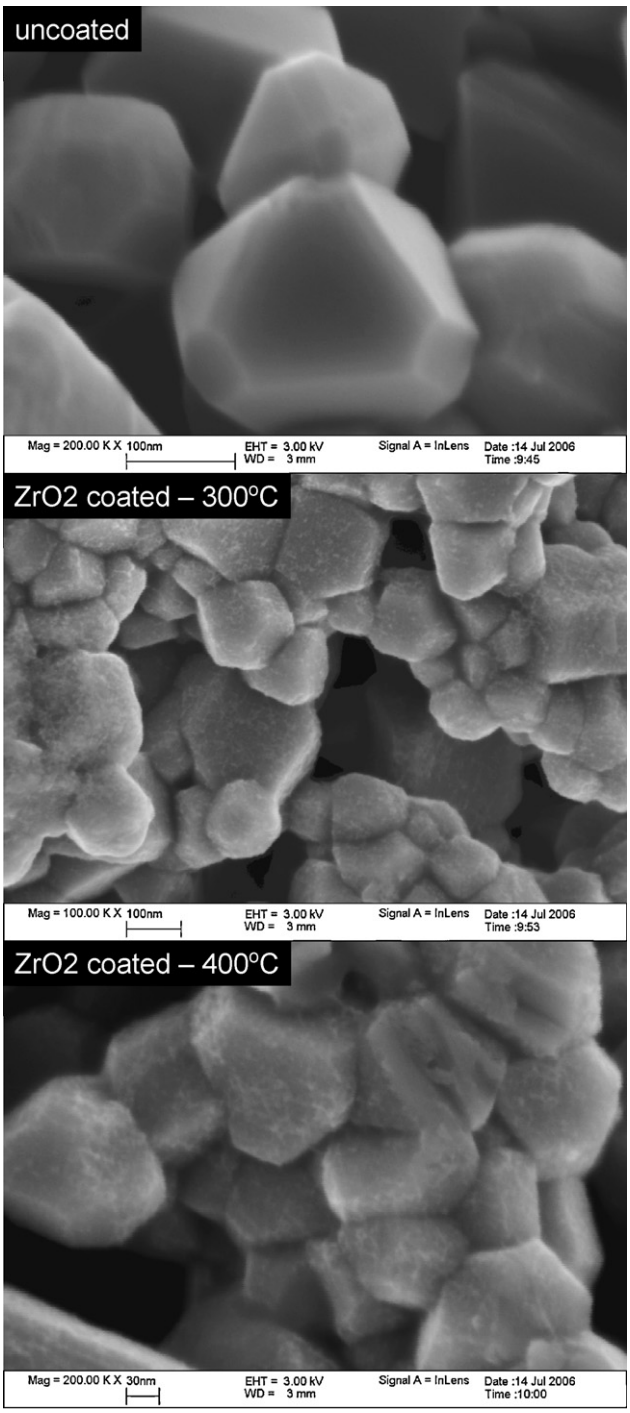

Fig. 4. SEM images of ZrO_2-coated $LiMn_2O_4$ electrode laminates fired at 300 and 400 °C.

carbonate based electrolytes is typically reported as about 0.42 nm [61–63].Scanning electron microscopy (SEM) confirmed that the sol–gel deposition process successfully coated the $LiMn_2O_4$ spinel particles with both ZrO_2 and TiO_2 (Fig. 3). Uncoated spinel crystals with well defined facets were easily observed at a magnification of 20,000×. By contrast, the facets of the coated spinel crystals were obscured. Inspection at higher magnifications of 50,000× showed that the ZrO_2 and TiO_2 coatings were heterogenous. In each case, it appeared that the sol–gel process had coated some spinel particles more extensively than others, the coating thickness varying from a thin layer in some instances to dense aggregates in others.

Our previous studies at the University of Wisconsin have shown that the ZrO_2 sol–gel product transforms from an amorphous state to a tetragonal crystalline structure when fired at 400 °C in air, and that sintering, first at 300 °C and then at 400 °C, increased the mean pore size from 0.7 to 1.9 nm, respectively, to form a porous ZrO_2 network [54]. SEM images of ZrO_2-coated spinels fired at these two temperatures, obtained at a 200,000× magnification showed little physical differences in coating morphology (Fig. 4). BET adsorption measurements showed that the surface area of the uncoated spinel was 4.5 $m^2\ g^{-1}$, whereas the surface area of the ZrO_2-coated spinel product after firing at 300 °C was 6.2 and 4.7 $m^2\ g^{-1}$ after further sintering at 400 °C. A preliminary analysis of the average pore

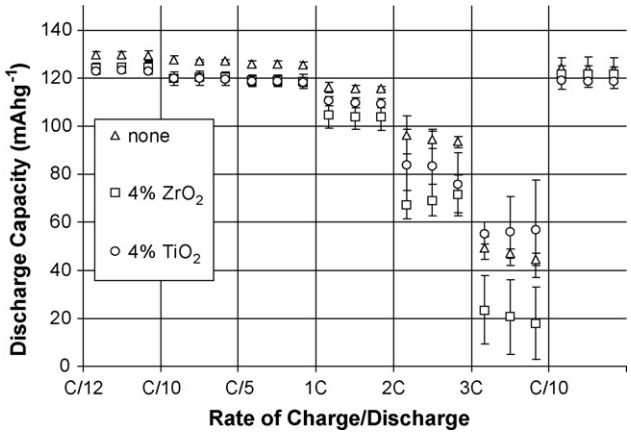

Fig. 5. Capacity of TiO_2- and ZrO_2-coated $LiMn_2O_4$ electrodes as a function of current rate. Each set of cells ($n = 6$) was cycled three times at each rate step. Symbols represent mean discharge capacities and error bars represent standard deviations. Note the superior capacity of the TiO_2 (circles) relative to the ZrO_2 (squares) at rates of 1 C and above.

diameters from the adsorption and desorption branches of the BET isotherms using the Barrett et al. method [64] suggested that the ZrO_2 coating fired at 300 °C had narrower pores than the coating heated at 400 °C, however the measures obtained were somewhat obscured by the large contribution of numerous pores falling below the lower limits of the BJH model for the 300 °C coating.

3.2. Room temperature rate capability

When cycled at a C/10 rate, the ZrO_2- and TiO_2-coated $LiMn_2O_4$ electrodes that had been fired at 400 °C delivered a slightly lower capacity than an uncoated electrode, providing mean capacities of ~120 and ~127 mAh g^{-1}, respectively (Fig. 5). This result is expected because the coating process added 4% of electrochemically inert material to the active spinel component. When cycled progressively at higher rates, the discharge capacity of all the cells decreased, those with ZrO_2-coated electrodes showing the most severe effect. Multiple tests were conducted on cells with ZrO_2- and TiO_2-coated electrodes and an uncoated $LiMn_2O_4$ 'control' electrode (six of each) to confirm the reproducibility of the experiments, from which average capacities and standard deviations were determined (Table 1). For cycling rates of 1 C or higher, the capacity of TiO_2-coated electrodes was always higher than that of the ZrO_2-coated electrodes. We suspect that the superior performance of the TiO_2-coated electrodes relative to that of the ZrO_2-coated electrodes may result from a more optimal pore size distribution and faster Li^+-ion transport through the coating. At discharge rates of 2 and 3 C, the TiO_2-coated electrodes had mean discharge capacities that were similar to that of the uncoated control spinel. In fact, when discharged at 3 C, the TiO_2-coated electrodes exhibited a mean discharge capacity that was actually higher than that of the uncoated material, however due to the magnitude of the standard deviation of the mean, this difference should not be considered statistically significant (t-test statistics: $t = 1.73$, DF = 10, $p = .115$). When cycled at the highest 3 C rate, it was also observed that the standard deviation for both ZrO_2- and TiO_2-coated electrodes was considerably larger than that of the uncoated control (Table 1). We

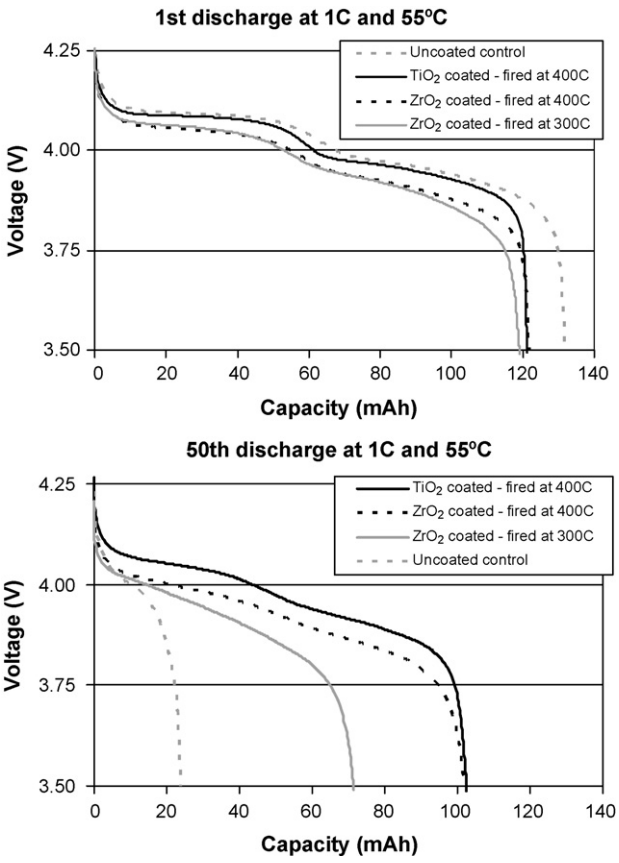

Fig. 6. Discharge profiles of the 1st and 50th cycles of lithium cells with coated and uncoated $LiMn_2O_4$ electrodes cycled at 1 C at 55 °C.

speculate that this variance is due to the heterogeneous nature of the sol–gel coatings, and physical non-uniformity amongst the coated electrodes. An opportunity exists for future work in this area to develop alternative coating deposition methods that might address and limit this variability.

3.3. Elevated temperature stability

To examine performance under both moderate power and thermal stress, coated electrodes were subjected to 50 cycles at a rate of 1 C at 55 °C. Both TiO_2 and ZrO_2 coatings showed significant improvements relative to the uncoated spinel (Fig. 6). For the uncoated cells, capacity fade at 55 °C was clearly evident after only 10 cycles, becoming progressively more severe with each cycle (Fig. 7). After 50 cycles, the mean capacity for the uncoated spinels had been reduced by more than 60%. The variance of the control cells also increased, which is evident from the large error bars in the later cycles. Both the TiO_2- and the ZrO_2-electrodes that had been fired at 400 °C showed superior stability, demonstrating capacity losses limited to ~10%. By comparison, ZrO_2 electrodes fired at 300 °C showed only a moderate improvement in their stability relative to the uncoated electrodes. We attribute the inferior performance of ZrO_2 coatings fired at the lower temperature to a narrower pore size distribution, thereby limiting Li^+-ion transport. To further

Table 1
Mass specific discharge capacity of coated $LiMn_2O_4$ electrodes. Mean values are reported in mAh g^{-1} with standard deviations in parentheses ($n = 6$ for each coating type).

Costing	C/10	C/5	1 C	2 C	3 C	C/10 (post)
None	127.15(1.03)	125.65(1.01)	115.78(1.34)	94.57(4.62)	47.04(3.50)	126.10(0.65)
4%TiO_2	119.71 (2.49)	118.35(1.84)	109.71 (1.91)	80.78(13.72)	56.23(12.56)	118.34(2.34)
4%ZiO_2	120.14(1.11)	118.97(2.22)	104.04(4.93)	69.22(6.48)	20.72(13.70)	124.57(2.90)

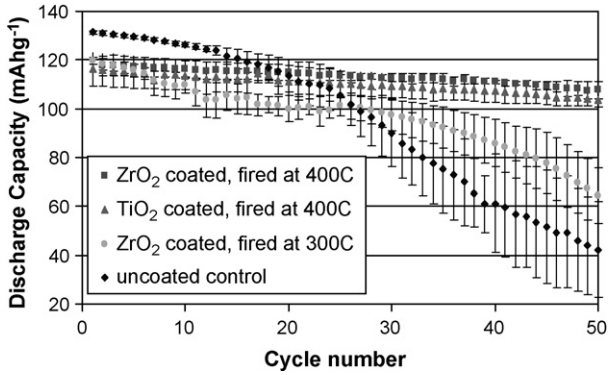

Fig. 7. Comparison of sol–gel coated $LiMn_2O_4$ electrodes with an uncoated $LiMn_2O_4$ control electrode cycled at a 1 C rate at 55 °C.

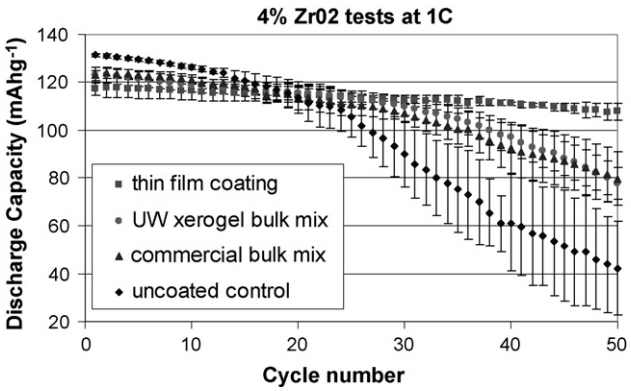

Fig. 9. Comparison of ZrO_2-coated $LiMn_2O_4$ electrodes with composite $ZrO_2/LiMn_2O_4$ electrodes cycled at a 1 C rate at 55 °C.

investigate the effect of firing temperature on the ZrO_2 coatings, a series of cells was cycled at a 3 C rate at 55 °C. Although all the cells lost capacity steadily, the ZrO_2-coated electrodes (400 °C) provided the most stable cycling behavior, confirming the superiority of these coated electrodes (Fig. 8).

In our earlier studies, we commented on the ability of ZrO_2 coatings to neutralize hydrofluoric acid generated from the hydrolysis of the $LiPF_6$ electrolyte salt [45,46]. It was suggested that the ZrO_2 might scavenge HF by forming various types of oxonium-zirconium-fluoride hydrate structures such as $ZrF_5^- \cdot H_3O^+ \cdot 2H_2O$ (alternatively, $ZrO_2 \cdot 5HF \cdot H_2O$). To further test this hypothesis, $LiMn_2O_4$ spinel electrodes containing a 4% composite mixture of commercial submicron ZrO_2 were cycled at 1 C. Composite electrodes containing a mixture of $LiMn_2O_4$ and 4% of ZrO_2 colloidal nanoparticles were also evaluated to differentiate between HF scavenging effects of independent ZrO_2 colloidal nanoparticles in the mixed composite electrode and stability enhancement due to the ZrO_2 coatings (Fig. 9). As shown, the stability of the mixed composite $LiMn_2O_4/ZrO_2$ electrode is superior to the uncoated $LiMn_2O_4$ control electrode but inferior to the ZrO_2-coated electrodes. We attribute the improvement of the composite cathode relative to the $LiMn_2O_4$ control to the HF scavenging mechanism previously described. Comparing the two composite $LiMn_2O_4/ZrO_2$ electrodes, the average capacity for the $LiMn_2O_4$/colloidal ZrO_2 mixture was slightly higher than that of the $LiMn_2O_4$/submicron (commercial) ZrO_2 mix for most cycles, but this difference was not statistically significant given the large standard deviations among the cells.

The marked difference in the electrochemical performance of the ZrO_2-coated and composite $LiMn_2O_4/ZrO_2$ electrodes appears to be due to more than a simple scavenging of HF from the electrolyte. We propose that the porous network of the coatings serves to moderate transport of Li^+ ions, smoothing out the current density at the surface of the $LiMn_2O_4$ spinel particles. Electrochemical cells that undergo numerous charge/discharge cycles require a uniform current distribution to prevent localized depletion of the active electrode materials and localized accumulation of parasitic by-products [65]. When two lithium-ions approach a $LiMn_2O_4$ spinel cathode in rapid succession, i.e., at a high rate, the primary Li^+-ion current will concentrate typically on naturally occurring surface defects. If the second ion arrives before the first has time to diffuse into the spinel lattice, localized formation of over-discharge Mn(III) product may occur, resulting in subsequent capacity loss [24]. Thin film coatings, however, may serve to smooth the lithium current density, creating a secondary current distribution. We speculate that, as the Li^+ ions diffuse through the coating, they encounter a tortuous porous network with numerous twists, turns, dead ends and split paths. The likelihood of two ions moving through the thin film and sequentially impinging upon the same surface location of the spinel is decreased, thereby homogenizing the current distribution, preventing localized over-discharge, and reducing capacity fade.

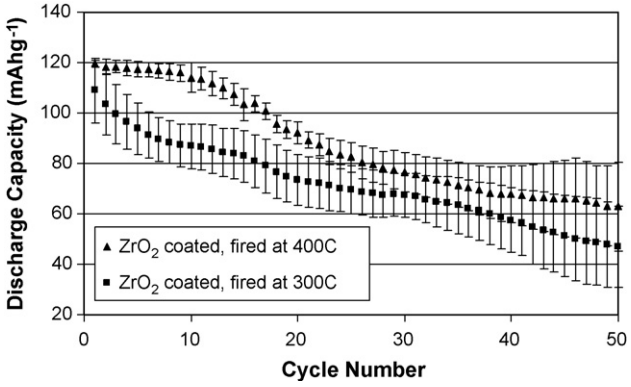

Fig. 8. Comparison of ZrO_2-coated $LiMn_2O_4$ electrodes cycled at a 3 C rate at 55 °C.

The mechanism proposed above is consistent with the observed performance of the TiO_2 coatings. TiO_2 reacts with hydrofluoric acid to form $TiOF_2 \cdot H_2O$ [66,67] (alternatively, $TiO_2 \cdot 2HF$) and therefore also serves to scavenge HF from the electrolyte. TiO_2 has an isoelectric point near that of ZrO_2 [68], and presenting a surface that is only slightly less basic [69]. It can be expected that the porous network created by the TiO_2 coatings should also be functionally similar to that of ZrO_2, serving to smooth the Li^+ ion current distribution and enhancing the stability of the $LiMn_2O_4$ electrode surface. The small differences (<5%) between the 400 °C fired ZrO_2 and TiO_2 coatings can likely be attributed to a combination of the minor differences in the acid–base surface chemistry and the variability in the nanoporous surface coatings.

3.4. Impedance analysis

In order to further elucidate the function of the ZrO_2 and TiO_2 coatings, impedance spectroscopy was used to probe both the resistive and capacitive behavior of the electrodes and their coatings. In our earlier studies of coated $LiMn_2O_4$ electrodes, we demonstrated that the impedance of the cells depended both on the chemical composition of the coating and the state of charge [46]. In the present study, this analysis was expanded to examine $LiMn_2O_4$ electrodes, both before and after 50 cycles at 55 °C at a 1 C rate.

A generalized equivalent circuit impedance model is shown in Fig. 10 that is useful for interpreting spectra. The Nyquist plot includes the real (resistive) component of the impedance on the horizontal axis, and the imaginary (capacitive) component of the impedance on the vertical axis. The axes have been shifted to facili-

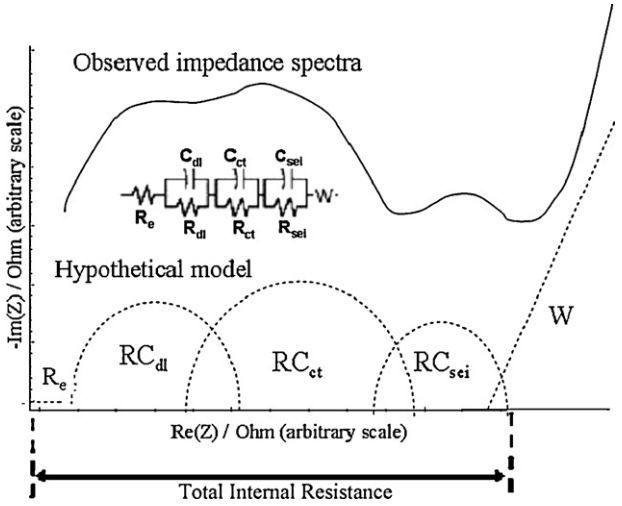

Fig. 10. Measured impedance spectra and proposed equivalent circuit model for a freshly assembled cell with a ZrO_2-coated $LiMn_2O_4$ electrode.

tate comparison of the measured spectra with the equivalent circuit schematic and modeled spectra. The impedance response is partitioned into contributions from several different components. The first is the electrolyte or solution resistance (R_e). This is followed by three pairs of resistor and capacitor elements arranged in parallel that represent the electric double layer (RC_{dl}), charge-transfer at the spinel surface (RC_{ct}), and the solid electrolyte interface layer (RC_{sei}). Finally, a Warburg element (W) is used to model semi-infinite diffusion in the bulk cathode material. Of primary interest is the total internal resistance of the cell, which is represented by the sum of the real components of the impedance extending along the horizontal axis.

4. Uncoated $LiMn_2O_4$ electrodes

Fig. 11 shows the impedance spectra for a representative cell containing the uncoated $LiMn_2O_4$ control electrode. Before cycling, the impedance was small and reached its lowest value at full charge of the cell. The total internal resistance varied from about 15 to 20 Ω. By comparison, after fifty 1 C cycles at 55 °C the impedance of the uncoated $LiMn_2O_4$ electrode increased by more than an order of magnitude. We attribute the substantial low frequency impedance increase to the formation of a detrimental solid electrolyte interfacial layer at the spinel surface. We speculate that the high temperature treatment resulted in excessive disproportionation of Mn(III) into Mn(II) and Mn(IV). Dissolution of the manganese II oxide (MnO) and generation of the manganese IV oxide (MnO_2) at the surface would impede the conductive pathways for lithium-ions entering the spinel. It is also interesting to note that, after cycling, the impedance of the control cells at full state of charge (4.3 V) was higher than at lower states of charge. The impedance values at 4.3 V were also the most variable of all measurements taken, the magnitude of which corresponded with the 1 C cycling performance of the control cells. This result is a good indication that the observed changes in impedance are due to chemical changes at the cathode surface, rather than manifestations of poisoning phenomena brought about by the migration and deposition of soluble Mn(II) at the graphitic anode of lithium-ion cells.

5. ZrO_2-coated electrodes

Fig. 12 shows the impedance spectra for a representative cell containing a ZrO_2-coated $LiMn_2O_4$ electrode fired at 300 °C. Fresh cells prior to cycling showed an increase in impedance relative to

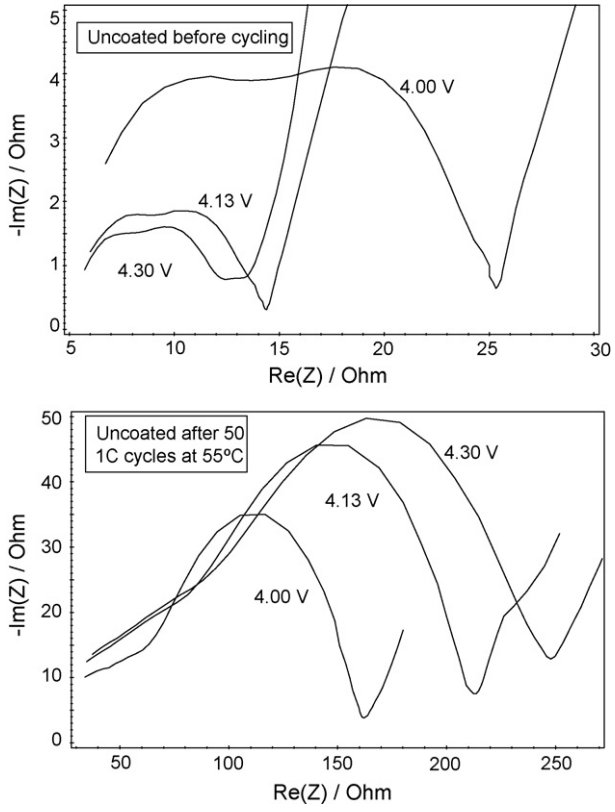

Fig. 11. Impedance spectra for an uncoated $LiMn_2O_4$ electrode.

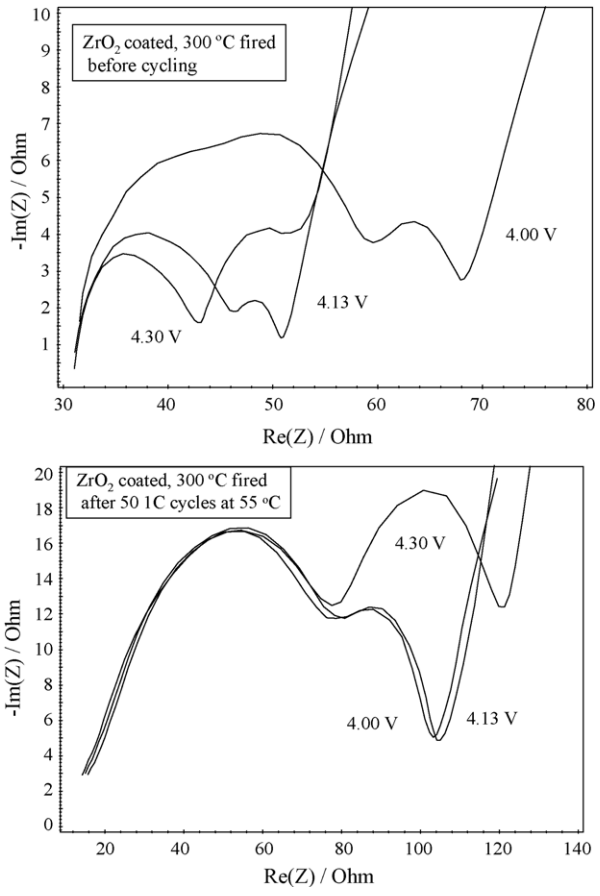

Fig. 12. Impedance spectra for a ZrO_2-coated $LiMn_2O_4$ electrode fired at 300 °C.

Table 2
Internal resistance data for cells after cycling 50 times at a 1 C rate at 55 °C. Mean values reported with standard deviations in parentheses ($n = 3$ for each cathode type).

Cathode chemistry	R_{int} @ 4.00 V (Ohm)	R_{int} @ 4.14 V (Ohm)	R_{int} @ 4.30 V (Ohm)
Uncoated control	168 (31)	174 (59)	162 (79)
ZrO_2-coated, fired at 300 C	110 (10)	113 (15)	125 (20)
ZrO_2-coated, fired at 400 C	80 (33)	77 (28)	78 (26)
TiO_2-coated, fired at 400 C	81 (30)	74 (28)	72 (28)

the uncoated spinel. The spectra clearly showed more prominent contributions from the third low frequency RC element, which we attribute to the modified SEI layer formed by the coatings. The internal resistance of freshly-coated ZrO_2 electrodes fired at 300 °C was roughly double that of the uncoated spinel electrode, which is likely due to limitations of Li^+-ion transport through the coating. This observation is consistent with the slightly reduced potential and capacity of the coated electrodes on the first 1 C discharge profile (Fig. 6). However, the impedance rise of these ZrO_2-coated $LiMn_2O_4$ electrodes upon 1 C cycling at 55 °C (50 cycles) was not as severe as it was for the uncoated control electrode (Table 2); these data emphasize the beneficial effect that the coatings have on improving the stability of the spinel electrode surface to electrochemical cycling. The overall lower internal resistance of cells with ZrO_2-coated $LiMn_2O_4$ electrodes is consistent with their slightly improved 1 C cycling capacity compared to the uncoated control spinel electrode (Figs. 6 and 7).

Fig. 13 shows the impedance spectra for a representative cell containing a ZrO_2-coated $LiMn_2O_4$ electrode fired at 400 °C. The higher firing temperature slightly reduced the initial impedance of the fresh cells, and decreased the prominence of the RC_{sei} element associated with the coating. This agrees well with BET measurements, indicating that the higher firing temperature resulted in larger pore sizes that would be more conducive to Li^+ ionic transport, hence lowering the overall impedance of the SEI component. After 1 C cycling at 55 °C, the internal resistance of these cells roughly doubled, but remained significantly lower than that of cells with uncoated $LiMn_2O_4$ electrodes and those fired at 300 °C. Our interpretation of the impedance spectra is consistent with that of others, who showed that a mid-frequency impedance arc resulted from a series of processes at the solid electrolyte interface, resulting in an increased resistance to Li^+-ion transport through the surface film [70].

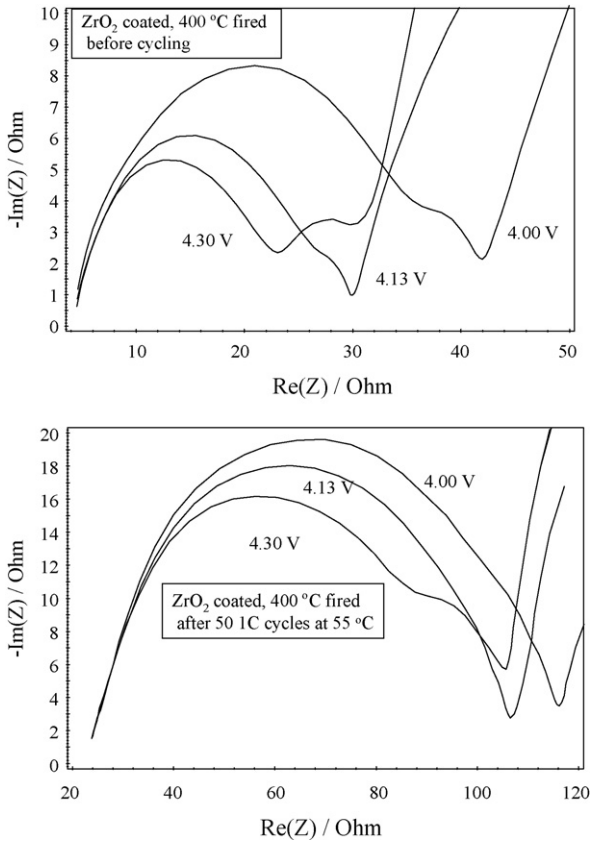

Fig. 13. Impedance spectra for a ZrO_2-coated $LiMn_2O_4$ electrode fired at 400 °C.

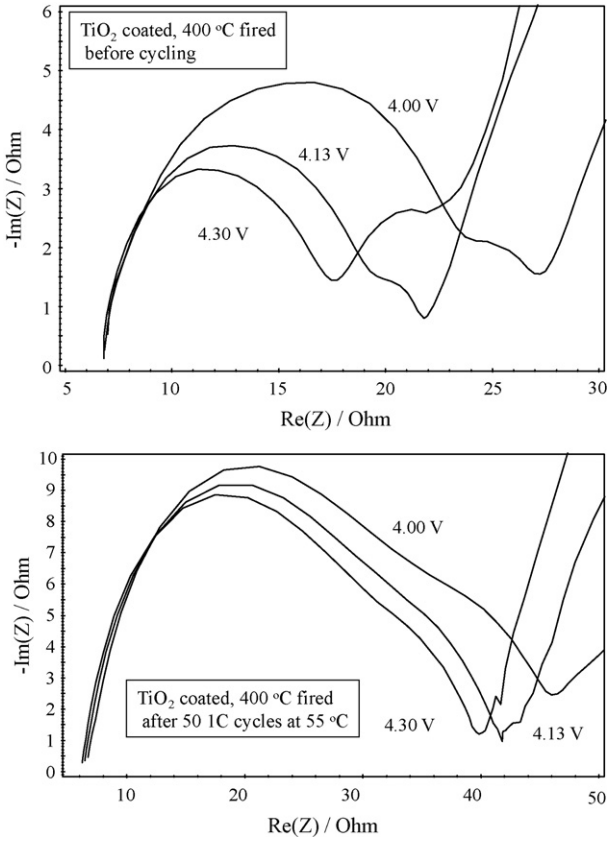

Fig. 14. Impedance spectra for a TiO_2-coated $LiMn_2O_4$ electrode fired at 400 °C.

6. TiO_2-coated $LiMn_2O_4$ electrodes

Fig. 14 shows the impedance spectra for a representative cell containing a TiO_2-coated $LiMn_2O_4$ electrode fired at 400 °C. The spectra show the same trends as ZrO_2-coated electrodes that had been fired at the same temperature; however, the TiO_2-coated electrodes showed slightly smaller impedance values. This effect is tentatively attributed to the larger TiO_2 particles (4.8 nm), which are expected to yield larger pores in the coatings than the smaller ZrO_2 particles (3.3 nm). Upon cycling, the impedance of the TiO_2-coated $LiMn_2O_4$ electrodes increased modestly (Fig. 14), with the internal cell resistances ranging from 50 to 70 Ω (Table 2); the resistance at the top of charge (4.3 V) remained lower than that obtained at other voltages, even after cycling (Fig. 14).

Although the impedance values measured after high temperature cycling were highly variable, the results for the TiO_2- and ZrO_2-coated electrodes fired at 400 °C are particularly noteworthy because the average internal resistance values are less than half that of the uncoated spinel electrode (Table 2). We accredit the superior 1 C high temperature cycling capacity of the TiO_2- and ZrO_2-coated electrodes to the protection of the $LiMn_2O_4$ surface and the rela-

tively low impedance imparted by the coatings. These results are consistent with related studies in which it was demonstrated that nanoparticulate metal oxide coatings applied to 5-V spinel electrodes improved both cycling performance and rate capability at high temperatures by suppressing the formation of thick SEI layers and enhancing charge-transfer kinetics [71,72].

7. Conclusions

This study has demonstrated that the stabilizing effect of nanoporous ZrO_2 and TiO_2 coatings on $LiMn_2O_4$ electrodes appears to result predominantly from two distinct processes: (1) neutralization of HF, which suppresses the acid attack of, and damage to, the $LiMn_2O_4$ electrode and (2) a more uniform current distribution provided by the nanoporous coating at the $LiMn_2O_4$ particle surface. The effect of firing temperature on pore size has been demonstrated for ZrO_2 coatings, and the superior cycling stability and discharge performance of coated electrodes has been shown to result from greatly reduced electrochemical impedance. Further work is required to investigate and tailor the surface properties of other amphoteric metal oxide coatings such as MgO, ZnO and Al_2O_3 to find the optimum material for optimizing the electrochemical properties and long-term cycling stability of $LiMn_2O_4$ spinel electrodes.

While the ZrO_2 and TiO_2 coatings were only applied to stoichiometric $LiMn_2O_4$ spinel electrodes, the benefits offered by nanoporous thin films may prove useful for other cathode chemistries such as high capacity, layered lithium-mixed-metal-oxides that require a charging potential (4.6 V) and the family of 5 V spinels [73]. If developed on a commercial scale, such nanofabrication techniques may offer an attractive option for implementing significant improvements in lithium-ion battery performance and lifetime.

Acknowledgments

Jennifer Jackowski assisted in the preparation of this manuscript. Isabel Tejedor, Louise Tortorelli, Amy Suyama and Wendy Suyama were instrumental in the development and preparation of ZrO_2 and TiO_2 coating materials. Kevin Lauzze and Jeom-Soo Kim provided assistance in the preparation of cathode laminates and lithium battery assembly. Financial support for MMT and CSJ from the Office of Vehicle Technologies of the U.S. Department of Energy under Contract No. DE-AC02-06CH11357 is gratefully acknowledged.

References

[1] A. Nagarkatti, Trans. Soc. Adv. Electrochem. Sci. Technol. 36 (1) (2002) 1–8.
[2] R. Hahn, J. Mueller, Proceedings of Electronics Goes Green, Fraunhofer IZM, Berlin, Germany, 2000, pp. 727–734.
[3] R.M. Dell, Solid State Ionics 134 (2000) 139–158.
[4] B.B. Owens, W.H. Smyrl, J.J. Xu, J. Power Sources 81 (1999) 150–155.
[5] L. King, Ind. Miner. 447 (2004) 45–51.
[6] T.E. Graedel, Chemical Compounds in the Atmosphere, Academic Press, New York, 1978.
[7] F.A. Cotton, G. Wilkinson, Advanced Inorganic Chemistry, Interscience, New York, 1972.
[8] M.M. Thackeray, W.I.F. David, P.G. Bruce, J.B. Goodenough, Mater. Res. Bull. 18 (1983) 461–472.
[9] A.D. Robertson, S.H. Lu, W.F. Averill, W.F. Howard, J. Electrochem. Soc. 144 (10) (1997) 3500–3505.
[10] Z. Zhang, D. Fouchard, J.R. Rea, J. Power Sources 70 (1) (1998) 16–20.
[11] A.N. Jansen, A.J. Kahaian, K.D. Kepler, P.A. Nelson, K. Amine, D.W. Dees, D.R. Vissers, M.M. Thackeray, J. Power Sources 81–82 (1999) 902–905.
[12] S. Tobishima, K. Takei, Y. Sakurai, J. Yamaki, J. Power Sources 90 (2) (2000) 188–195.
[13] S. Tobishima, K. Hayashi, K. Takei, M. Takahashi, Y. Sakurai, Key Eng. Mater. 216 (2002) 111–114.
[14] D.R. Sadoway, A.M. Mayers, Mater. Res. Soc. Bull. 8 (2002) 590–596.
[15] Y. Baba, S. Okada, J. Yamaki, Solid State Ionics 148 (2002) 311–316.
[16] Y.J. Kang, J.H. Kim, Y.K. Sun, J. Power Sources 146 (2) (2005) 140–237.
[17] Q. Luo, A. Manthiram, J. Electrochem. Soc. 156 (2) (2009) A84–A88.
[18] C.Q. Feng, H. Li, P. Zhang, Z.P. Guo, H.K. Liu, Mater. Chem. Phys. 119 (1–2) (2010) 82–85.
[19] P. Arora, R.E. White, J. Electrochem. Soc. 145 (10) (1998) 3647–3667.
[20] O. Hass, E.J. Cairns, R. Soc. Chem. Ann. Rep. Prog. Chem.—Sect. C: Phys. Chem. 95 (1999) 163–197.
[21] L.S. Kanevskii, V.S. Dubasova, Russ. J. Electrochem. 41 (1) (2005) 1–16.
[22] M.M. Thackeray, Prog. Solid State Chem. 25 (1) (1997) 1–71.
[23] R.J. Gummow, A. DeKock, M.M. Thackeray, Solid State Ionics 69 (1994) 59–67.
[24] M.M. Thackeray, Y. Shao-Horn, A.J. Kahanian, K.D. Kepler, E. Skinner, J.T. Vaughey, S.A. Hackney, Electrochem. Solid State Lett. 1 (1998) 7–9.
[25] K.A. Striebel, E. Sakai, E.J. Cairns, J. Electrochem. Soc. 149 (1) (2002) A61–A68.
[26] Y. Shin, A. Manthiram, J. Electrochem. Soc. 151 (2) (2004) A204–A208.
[27] Z. Chen, K. Amine, J. Electrochem. Soc. 153 (2) (2006) A316–A320.
[28] W. Choi, A. Manthiram, J. Electrochem. Soc. 153 (9) (2006) A1760–A1764.
[29] A. Du Pasquier, A. Blyr, P. Courjal, D. Lrcher, G. Amatucci, B. Gerand, J.M. Tarascon, J. Electrochem. Soc. 146 (2) (1999) 428–436.
[30] J. Cho, M.M. Thackeray, J. Electrochem. Soc. 146 (10) (1999) 3577–3581.
[31] T. Inoue, M. Sano, J. Electrochem. Soc. 145 (11) (1998) 3704–3707.
[32] H. Huang, C.A. Vincent, P.G. Bruce, J. Electrochem. Soc. 146 (2) (1999) 481–485.
[33] R. Premanand, A. Durairajan, B. Hara, R. White, B. Popov, J. Electrochem. Soc. 149 (1) (2002) A54–A60.
[34] L.F. Wang, C.C. Ou, K.A. Striebel, J.S. Chen, J. Electrochem. Soc. 150 (7) (2003) A905–A911.
[35] P. Ramadass, B. Haran, R. White, B. Popov, J. Power Sources 112 (2002) 606–613.
[36] D.H. Jang, Y.J. Shin, S.M. Oh, J. Electrochem. Soc. 143 (7) (1996) 2204–2211.
[37] Y. Matsuo, R. Kostecki, F. McLarnon, J. Electrochem. Soc. 148 (7) (2001) A687–A692.
[38] S.S. Zhang, K. Xu, T.R. Jow, J. Electrochem. Soc. 149 (12) (2002) A1521–A1526.
[39] R. Kosteki, Y. Matsuo, F. McLarnon, Lawrence Berkeley National Laboratory Publication LBNL-48362, 2001.
[40] H. Yamane, M. Saitoh, M. Sano, M. Fujita, M. Sakata, M. Takada, E. Nishibori, N. Tanaka, J. Electrochem. Soc. 149 (12) (2002) A1514–A1520.
[41] J. Cho, T.J. Kim, B. Park, J. Electrochem. Soc. 149 (3) (2002) A288–A292.
[42] A.M. Kannan, A. Manthiram, Electrochem. Solid State Lett. 5 (7) (2002) A167–169.
[43] Y.K. Sun, K.J. Hong, J. Prakash, J. Electrochem. Soc. 150 (7) (2003) A970–A972.
[44] J.M. Han, S.T. Myung, Y.K. Sun, J. Electrochem. Soc. 153 (7) (2006) A1290–A1295.
[45] M.M. Thackeray, C.S. Johnson, J.S. Kim, K.C. Lauzze, J.T. Vaughey, N. Dietz, D. Abraham, S.A. Hackney, W. Zeltner, M.A. Anderson, Electrochem. Commun. 5 (2003) 752–758.
[46] J.S. Kim, C.S. Johnson, J.T. Vaughey, S.A. Hackney, K.A. Walz, W.A. Zeltner, M.A. Anderson, M.M. Thackeray, J. Electrochem. Soc. 151 (10) (2004) A1755–A1761.
[47] Z. Liu, H. Wang, L. Fang, J.Y. Lee, L.M. Gan, J. Power Sources 104 (1) (2002) 101–107.
[48] A. Eftekhari, Solid State Ionics 167 (2004) 237–242.
[49] J.S. Gnanaraj, V.G. Pol, A. Gedanken, D. Aurbach, Electrochem. Commun. 5 (2003) 940–945.
[50] Y.M. Lin, H.C. Wu, Y.C. Yen, Z.Z. Guo, M.H. Yang, H.M. Chen, H.S. Sheu, N.L. Wu, J. Electrochem. Soc. 152 (8) (2005) A1526–A1532.
[51] C. Li, H.P. Zhang, L.J. Fu, H. Liu, Y.P. Wu, E. Rahm, R. Holze, H.Q. Wu, Electrochim. Acta 51 (2006) 3872–3883.
[52] Y. Wang, G. Cao, Adv. Mater. 20 (2008) 2251–2269.
[53] C.J. Brinker, G.W. Scherer, Sol–Gel Science: The Physics and Chemistry of Sol–Gel Processing, Elsevier Academic Press, London, 1990.
[54] Q. Xu, M.A. Anderson, J. Am. Ceram. Soc. 77 (7) (1994) 1939–1945.
[55] M.M. Thackeray, S.H. Kang, C.S. Johnson, J.T. Vaughey, R. Benedek, S.A. Hackney, J. Mater. Chem. 17 (2007) 3112–3125.
[56] S.H. Kang, M.M. Thackeray, Electrochem. Commun. 11 (2009) 748–751.
[57] S. Komaba, N. Kumagai, T. Sasaki, Y. Miki, Electrochemistry 69 (10) (2001) 784–787.
[58] S. Brunauer, P.H. Emmett, E. Teller, J. Am. Chem. Soc. 60 (1938) 309–319.
[59] R.K. McGeary, J. Am. Ceram. Soc. 44 (10) (1961) 513–522.
[60] M. Klotz, A. Ayral, C. Guizard, L. Cot, Bull. Korean Chem. Soc. 20 (8) (1999) 879–884.
[61] S. Tobishima, T. Okada, Electrochim. Acta 30 (1985) 1715–1722.
[62] R. Naejus, R. Coudert, P. Willmann, D. Lemordant, Electrochim. Acta 43 (3–4) (1998) 275–284.
[63] T. Li, P.B. Balbuena, J. Electrochem. Soc. 146 (10) (1999) 3613–3622.
[64] E.P. Barrett, L.S. Joyner, P.P. Halenda, J. Am. Chem. Soc. 73 (1951) 373–380.
[65] O. Lanzi, U. Landau, NASA Lewis Research Center Publication SEE N87-29914, 1987, pp. 24–44.
[66] Y.A. Buslaev, V.A. Bochkareva, N.S. Nikolev, Russ. Chem. Bull. 3 (1962) 388–392.
[67] J.H. Moss, G.D. Parfitt, A. Wright, Colloid Polym. Sci. 256 (1978) 1121–1130.
[68] J. Nawrocki, M.P. Rigney, A. McCormick, P.W. Carr, J. Chromatogr. A 657 (1993) 229–282.
[69] C. Sun, J.C. Berg, Adv. Colloid Interface Sci. 105 (2003) 151–175.
[70] D.P. Abraham, E.M. Reynolds, P.L. Schultz, A.N. Jansen, D.W. Dees, J. Electrochem. Soc. 153 (8) (2006) A1610–A1616.
[71] J. Liu, A. Manthiram, J. Electrochem. Soc. 156 (1) (2009) A66–A72.
[72] J. Liu, A. Manthiram, J. Electrochem. Soc. 156 (9) (2009) A709–A719.
[73] C.S. Johnson, N.C. Li, C. Lefief, J.T. Vaughey, M.M. Thackeray, Chem. Mater. 20 (19) (2008) 6095–6106.